Rotor Time Constant Estimation of Induction Motors Using Phase Responses During I-F Operations

Ho-Ryul Park, *Student Member, IEEE*, Yun-Jai Oh, Seok-Min Bae, Seung-Cheol Choi, Myung-Seop Lim, *Senior Member, IEEE*, and Young-Doo Yoon, *Senior Member, IEEE*

***Abstract*—This article proposes a method for estimating induction motors' (IMs') rotor time constant (RTC). An accurate estimation is needed since RTC is an essential motor parameter for high-performance operation. As the RTC changes due to magnetic saturation, the magnetic saturation of magnetizing flux is considered. The proposed method estimates the RTC during the I-F operation, which is robust to the stator resistance error, under a no-load state considering the sensorless motor drive system. This article analyzes the response of the rotor magnetic flux to the stator current in a stator current-oriented coordinate. The proposed method estimates RTC through the phase response of the rotor magnetic flux to the stator current. As a result of analyzing the method based on magnitude and phase responses, the method based on phase response is more robust against errors of motor parameters in the proposed algorithm. The proposed method is verified through computer simulation and experiment with 3.7 and 11 kW IMs.**

***Index Terms*—Frequency response, induction motor (IM), parameter estimation, rotor time constant (RTC).**

NOMENCLATURE

$\mathbf{J} = \begin{bmatrix} 0 & -1 \\ 1 & 0 \end{bmatrix}$	orthogonal rotation matrix.
$f_s^{\omega} = \begin{bmatrix} f_{ds}^{\omega} & f_{qs}^{\omega} \end{bmatrix}^{\mathrm{T}}$	d-q axis representation of stator at the arbitrary synchronous reference frame ω.
$f_r^{s} = \begin{bmatrix} f_{dr}^{s} & f_{qr}^{s} \end{bmatrix}^{\mathrm{T}}$	d-q axis representation of rotor at the stationary reference frame.
$\mathbf{V}_s = \begin{bmatrix} V_{ds} & V_{qs} \end{bmatrix}^{\mathrm{T}}$	d-q axis stator voltage.
$\mathbf{i}_s = \begin{bmatrix} i_{ds} & i_{qs} \end{bmatrix}^{\mathrm{T}}$	d-q axis stator current.
$\boldsymbol{\lambda}_s = \begin{bmatrix} \lambda_{ds} & \lambda_{qs} \end{bmatrix}^{\mathrm{T}}$	d-q axis stator magnetic flux.
R_s	stator resistance.
L_s	stator inductance.
L_m	magnetizing inductance.
L_{ls}	stator leakage inductance.
ω_r	rotor angular velocity.
σL_s	transient inductance.
τ_r	rotor time constant.
$A \equiv B$	define A as B.
$\|\|\cdot\|\|_{ac}$	ac component magnitude.

Manuscript received 26 January 2024; revised 13 April 2024 and 26 June 2024; accepted 17 July 2024. Date of publication 28 August 2024; date of current version 14 February 2025. This work was supported by the National Research Foundation of Korea (NRF) under grant funded by the Korea government (MSIT) (No. RS-2023-00207865). *(Corresponding author: Young-Doo Yoon.)*

Ho-Ryul Park and Yun-Jai Oh are with the Department of Automotive Engineering (Automotive-Computer Convergence), Hanyang University, Seoul 133-791, South Korea (e-mail: phrtiger@hanyang.ac.kr; automaker@hanyang.ac.kr).

Seok-Min Bae is with the Department of Automotive Engineering (Future Mobility), Hanyang University, Seoul 133-791, South Korea (e-mail: bemynn97@hanyang.ac.kr).

Seung-Cheol Choi, Myung-Seop Lim, and Young-Doo Yoon are with the Department of Automotive Engineering, Hanyang University, Seoul 133-791, South Korea (e-mail: dumpalcu@hanyang.ac.kr; myungseop@hanyang.ac.kr; yoonyd@hanyang.ac.kr).

Digital Object Identifier 10.1109/TIE.2024.3436606

I. INTRODUCTION

SINCE induction motors (IMs) are inexpensive, structurally robust, and have low maintenance costs, IMs are widely used across industrial applications. Recently, IMs have been used even for high performance with the control algorithm development [1], [2], [3], [4], [5], [6], [7]. The rotor time constant (RTC) represents the characteristics of the IMs and is an important parameter used in indirect or direct flux-oriented control (IFOC or DFOC).

The parameters of IM fluctuate depending on the temperature, input frequency, and magnetic flux saturation. The parameters greatly affected by the motor's temperature are the stator and rotor resistances. As the motor temperature rises, the stator and rotor resistance increases. Also, in IMs, slip occurs due to the difference between the speed of the magnetic field and the rotor speed. Depending on the magnitude of the slip frequency, the current density varies in the depth of the conductor by the skin effect. Due to the skin effect, the rotor resistance increases, and the rotor leakage inductance decreases [8]. Lastly, the magnetic saturation is mainly caused by the stator current, which changes the stator leakage inductance and magnetizing inductance.

As mentioned earlier, parameter changes can degrade IMs' instantaneous torque control performance. However, in general, the impact of the error in parameter on speed control performance is significantly reduced by the PI controller [9]. Therefore, the error in the parameters does not have a significant effect on the control system with rotor position or speed sensors. Besides, it is crucial to estimate the motor parameters accurately for sensorless operation. Sensorless vector control of the IM is mainly operated based on the motor model; inaccurate motor parameters cause speed errors and reduce stability [1], [2], [3], [4], [5]. The stator resistance is a crucial factor that causes IM's rotor flux position error [6]. Therefore, knowing the accurate stator resistance significantly impacts the IM sensorless

performance. Accordingly, sensorless algorithms that change stator resistance adaptively online have been proposed [5], [6], [7].

Depending on whether the rotor rotates during the estimation process, the motor parameter estimation techniques can be classified into stationary and rotational techniques [10], [11], [12], [13], [14], [15]. The stationary parameter estimation technique is suitable for use in the initial self-commissioning of the motor because operators can identify the parameters without rotating the motor, even in limited situations. Additionally, it is easy to use in a sensorless system because it does not require rotor position or speed information. However, when the motor remains stationary, the voltage magnitude applied during the estimation process is comparatively low, so the inverter nonlinearity effect [16] appears significant, causing a sizeable parameter error.

For this reason, many stationary parameter estimation techniques have been proposed to minimize the impact of the inverter nonlinearity effect. A proposed method [10] constructs a voltage equation, including the voltage distortion component of the inverter, and cancels out during the estimation process. This method can guarantee an estimation performance even without compensating the nonlinearity of the inverter. In addition, [11] compensates the nonlinearity of the inverter by obtaining the relationship between voltage and current experimentally, and there are several methods to estimate the parameter using the inverter nonlinearity compensation method [12], [13].

In the case of the rotational parameter estimation technique, a relatively high voltage can be applied to the inverter compared with the stationary parameter estimation technique. The higher voltage diminishes the portion of nonlinear voltage. Therefore, it has the advantage of reducing the errors due to the inverter voltage nonlinearity [17].

The RTC determines the dynamic characteristics of the IM. Additionally, it is a critical motor parameter because it is used to estimate the rotor flux position in IFOC and represents the IM model in sensorless algorithms. The RTC estimation method in control systems with position or speed sensors is done by analyzing the IM model [18], [19]. In [18], the RTC is calculated using a motor model after measuring the phase voltage, and in [19], it is estimated by designing an RTC compensator after analyzing the variance of RTC. Besides, since sensorless systems require accurate motor parameters for operation, they are often estimated online [6], [7]. In [6], stator resistance and rotor resistance were estimated sequentially using artificial neural network (ANN), and in [7], stator resistance and rotor resistance were estimated through signal injection. However, estimating RTC in model-based sensorless algorithms is complex and must inevitably be estimated with stator resistance. Therefore, the errors of the two parameters can be coupled.

If the I-F operation is used, RTC can be estimated without estimating the accurate stator resistance. The I-F operation is a scalar control that does not require speed feedback and allows open-loop speed control by changing the current frequency. Due to the characteristics of the rotor, the I-F operation of the IM is more accessible than that of the synchronous motor. Unlike FOC, I-F operation does not require precise knowledge of the rotor flux's position, so it is robust to the inaccuracy of the stator resistance.

This article proposes the rotational estimation method of the RTC of IMs. The proposed method is operated with I-F operation, considering the sensorless applications. Afterward, the d-axis current is injected as a sinusoidal alternating current (ac) signal on the direct current (dc) signal.

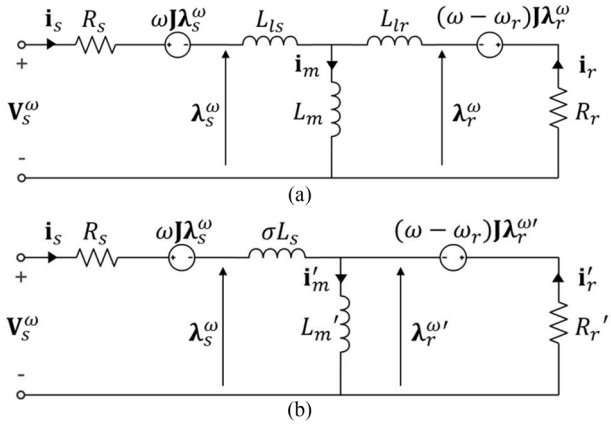

Fig. 1. Equivalent circuit models of IM. (a) T model. (b) Inverse Γ model.

The RTC is estimated under no-load condition, using the dynamic response of the rotor magnetic flux to the stator current. The magnitude response and phase response can be used to estimate the RTC. The magnetic saturation is considered, while RTC variances by rotor temperature and slip frequency are negligible, assuming the no-load state. The proposed method estimates the RTC based on the phase response. Generally, the signal's phase response is challenging to be obtained accurately because of phase extraction accuracy. The phase response is calculated based on the relationship between the stator and leakage magnetic flux. The two responses have different sensitivity to the errors during the estimation method. According to the sensitivity analysis, the proposed method is relatively more robust to the errors.

The stator magnetic flux is estimated in the proposed method through frequency adapted flux observer (FAO), [20]. Errors in the magnetic flux that occur using FAO are analyzed, and the estimated magnetic flux is compensated appropriately. The proposed method is verified with simulation and experiments.

This article was previously presented at the 2022 International Power Electronics Conference [21]; A detailed explanation and a method of estimating the RTC using the phase response are added, and additional comparison and analysis are presented.

II. Fundamental Equations of IMs

The equivalent circuits of the IMs are shown in Fig. 1. According to Fig. 1(a), the voltage equations at T model [22] of the IMs are expressed as

$$\mathbf{V}_s^{\omega} = R_s\mathbf{i}_s^{\omega} + \mathrm{s}\boldsymbol{\lambda}_s^{\omega} + \omega\mathbf{J}\boldsymbol{\lambda}_s^{\omega} \tag{1}$$

$$\mathbf{V}_r^{\omega} = R_r\mathbf{i}_r^{\omega} + \mathrm{s}\boldsymbol{\lambda}_r^{\omega} + (\omega-\omega_r)\mathbf{J}\boldsymbol{\lambda}_r^{\omega}. \tag{2}$$

The stator magnetic flux equation at T model of the IMs is expressed as

$$\boldsymbol{\lambda}_s^{\omega} = \sigma L_s\mathbf{i}_s^{\omega} + \frac{L_m}{L_r}\boldsymbol{\lambda}_r^{\omega}. \tag{3}$$

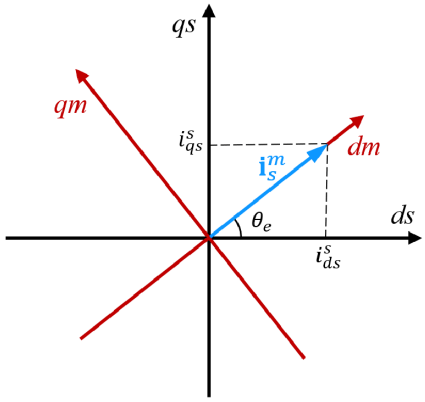

Fig. 2. Stator current-oriented coordinate.

The rotor current can be expressed as

$$\mathbf{i}_r^{\omega} = \frac{1}{L_r}\boldsymbol{\lambda}_r^{\omega} - \frac{L_m}{L_r}\mathbf{i}_s^{\omega} \tag{4}$$

from the relationship between the rotor magnetic flux and the currents. $\boldsymbol{\lambda}_r^{\omega} = L_r\mathbf{i}_r^{\omega} + L_m\mathbf{i}_s^{\omega}$.

Since the rotor voltage of the squirrel cage IMs is zero, the relationship between stator current and rotor magnetic flux is simply expressed as

$$\frac{R_r}{L_r}\boldsymbol{\lambda}_r^{\omega} - R_r\frac{L_m}{L_r}\mathbf{i}_s^{\omega} + \mathrm{s}\boldsymbol{\lambda}_r^{\omega} + (\omega - \omega_r)\mathbf{J}\boldsymbol{\lambda}_r^{\omega} = 0 \tag{5}$$

by substituting (4) to (2).

From (5), the rotor magnetic flux can be expressed by stator current as

$$\boldsymbol{\lambda}_r^{\omega} = \frac{L_m R_r}{L_r}\begin{bmatrix} s+\frac{R_r}{L_r} & -(\omega-\omega_r) \\ (\omega-\omega_r) & s+\frac{R_r}{L_r}\end{bmatrix}^{-1}\mathbf{i}_s^{\omega}. \tag{6}$$

Using (6) and (3), the stator magnetic flux is expressed with the stator current as

$$\boldsymbol{\lambda}_s^{\omega} = \begin{bmatrix} a & b \\ -b & a\end{bmatrix}\mathbf{i}_s^{\omega} \tag{7}$$

where $a = \sigma L_s + (L_m^2/L_r^2)R_r(s+(R_r/L_r))/((s+(R_r/L_r))^2 + (\omega-\omega_r)^2)$, $b = (L_m^2)/(L_r^2)R_r(\omega-\omega_r)/((s+(R_r)/(L_r))^2 + (\omega-\omega_r)^2)$.

In this article, we use a stator current-oriented coordinate that the stator current is on the d-axis, as shown in Fig. 2. In this coordinate system, the stator current is expressed as

$$\mathbf{i}_s^m = \begin{bmatrix} i_{ds}^m \\ i_{qs}^m\end{bmatrix} = \begin{bmatrix} i_s \\ 0\end{bmatrix}. \tag{8}$$

Assuming a no-load state ($\omega - \omega_r \approx 0$), (7) on the stator current-oriented coordinate can be simplified as

$$\boldsymbol{\lambda}_s^m = \begin{bmatrix}\lambda_{ds}^m \\ \lambda_{qs}^m\end{bmatrix} = \begin{bmatrix}\sigma L_s + \frac{L_m^2}{L_r}\frac{1}{\tau_r s+1} \\ 0\end{bmatrix} i_s\,. \tag{9}$$

From (9), the rotor magnetic flux in the inverse Γ model $\lambda_{dr}^{m'}$, as shown in Fig. 1(b), can be written as

$$\lambda_{dr}^{m'} = \lambda_{ds}^m - \lambda_\sigma = \frac{L_m^2}{L_r}\frac{\omega_c}{s+\omega_c}i_s \tag{10}$$

where the leakage magnetic flux $\lambda_\sigma = \sigma L_s i_s$, $\omega_c = 1/\tau_r$. And the relationship of the rotor magnetic flux between the T model and inverse Γ model is expressed as

$$\lambda_{dr}^m = \frac{1}{\gamma'}\lambda_{dr}^{m'} \tag{11}$$

where $\gamma' = L_m/L_r$.

From (10) and (11), λ_{dr}^m can be expressed as

$$\lambda_{dr}^m = \frac{1}{\gamma'}\left(\lambda_{ds}^m - \lambda_\sigma\right) = L_m\frac{\omega_c}{s+\omega_c}i_s. \tag{12}$$

Through (12), the response of the rotor magnetic flux to the stator current appears in the form of a first-order low-pass filter (LPF) with a cutoff frequency of ω_c.

III. Proposed Method

A. Proposed RTC Estimation

The proposed method controls the stator current in the I-F operation by injecting the ac signal $i_{ac}(s)$ into the dc signal I_{dc} as

$$i_s = I_{dc} + i_{ac}(s) \tag{13}$$

where $i_{ac}(s)$ is a sinusoidal signal with the magnitude I_{ac} and the operating angular frequency ω_o. By substituting (13) into (12), it can be represented as

$$L_m\frac{\omega_c}{s+\omega_c}\{I_{dc} + i_{ac}(s)\} = L_{m,app}\frac{\omega_c}{s+\omega_c}I_{dc} + L_{m,dyn}\frac{\omega_c}{s+\omega_c}i_{ac}(s) \tag{14}$$

where $L_{m,app}$ is an apparent inductance, and $L_{m,dyn}$ is a dynamic inductance.

Since the dc term refers to the operating point, it is expressed using $L_{m,app}$. Also, since the ac term refers to the small signal at the operating point, it is expressed using $L_{m,dyn}$.

From (12) and (14), the transfer function of the rotor magnetic flux for $i_{ac}(s)$ is obtained, and the magnitude response k is defined as

$$k \equiv \left|\frac{\lambda_{dr,ac}^m(s)}{i_{\mathrm{ac}}(s)}\right| = \frac{1}{\gamma'\,I_{ac}}\left|\left|\lambda_{ds,ac}^m - \lambda_{\sigma,ac}\right|\right|_{ac} \tag{15}$$

where subscript ac is ac component of the magnetic flux.

In addition, obtaining k from the transfer function [ac component of (14)] using ω_o and ω_c, k can be expressed as

$$k = L_{m,dyn}\frac{\omega_c}{\sqrt{\omega_o^2+\omega_c^2}}. \tag{16}$$

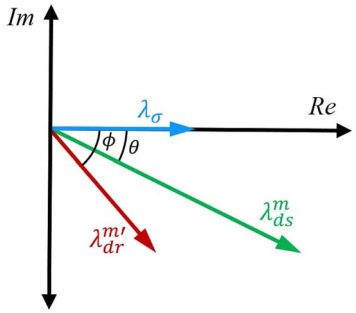

Fig. 3. Phasor diagram of the inverse Γ model on the stator current-oriented coordinate.

Since the proposed method extracts the ac signal of the stator current at the operating point, ω_c is the reciprocal of $\tau_{r,mag,dyn}$, which is defined as rotor dynamic inductance $L_{r,dyn}$ divided by R_r. Therefore, from (16), the estimated RTC $\tau_{r,mag,dyn}$ using k can be obtained as

$$\tau_{r,mag,dyn} = \frac{1}{\omega_c} = \frac{\sqrt{1-\left(k/L_{m,dyn}\right)^2}}{\left(k/L_{m,dyn}\right)\omega_o}. \tag{17}$$

Similarly, the phase response can be used to estimate the RTC. When calculating the phase difference between two sinusoidal signals, the results vary depending on the zero-crossing detection accuracy of the signals, so the phase difference is calculated using the magnitude of the magnetic flux vectors.

Since $\lambda^{m'}_{dr}$ and λ^{m}_{dr} have the same phase according to (11), the phase of λ^{m}_{dr} is calculated by the relationship of (10). Fig. 3 shows the phasor diagram of the magnetic flux in the inverse Γ model. The magnitudes of λ^{m}_{ds}, λ_σ, and $\lambda^{m'}_{dr}$ are denoted by A, B, and C. The phasor diagram in Fig. 3 is depicted with the reference phasor of λ_σ, because the phase of λ_σ obtained as the function of i_s ($\lambda_\sigma = \sigma L_s i_s$). Next, $\lambda^{m'}_{dr}$ appears as a first order LPF to i_s, as shown in (10). Therefore, $\lambda^{m'}_{dr}$ phase lags compared with i_s. And λ^{m}_{ds} is the sum of the others, as shown in (10). Consequently, as shown in Fig. 3, the phasor of λ^{m}_{ds} can be obtained by the sum of λ_σ and $\lambda^{m'}_{dr}$.

By using the law of cosines with the magnitude of the three magnetic fluxes, the phase of $\lambda^{m'}_{dr}$ can be obtained as

$$\phi = \cos^{-1}\left(\frac{A^2 - B^2 - C^2}{2BC}\right). \tag{18}$$

Like the magnitude response (16), obtaining ϕ from the first order transfer function at operating frequency ω_o, ϕ can be expressed as

$$\phi = \tan^{-1}\left(-\frac{\omega_o}{\omega_c}\right). \tag{19}$$

From (19), the dynamic RTC, reciprocal of ω_c, estimated in the phase method is calculated as

$$\tau_{r,phase,dyn} = \frac{1}{\omega_c} = \frac{\tan(\phi)}{\omega_o}. \tag{20}$$

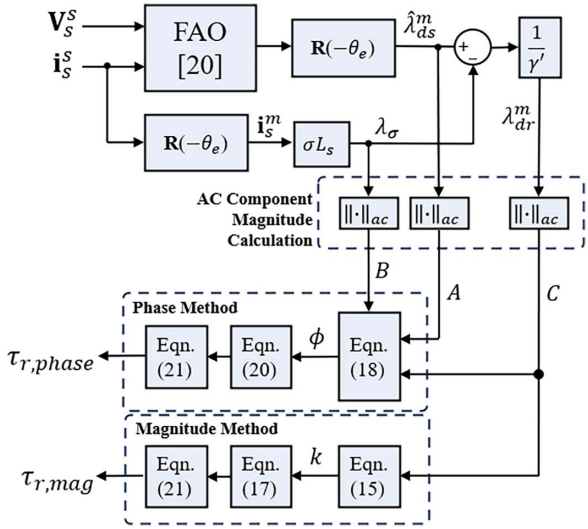

Fig. 4. Overall block diagram of the proposed method. $\mathbf{R}(-\theta_e)$ is the rotation matrix.

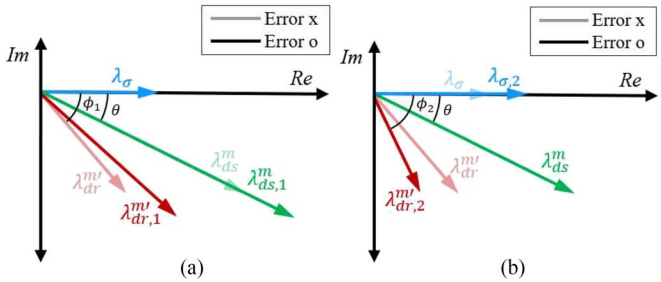

Fig. 5. Magnetic flux phasor diagram when estimation errors exist. (a) Stator magnetic flux error exists. (b) Transient inductance error exists.

Since the RTC required for vector control of IMs is the RTC using the apparent inductance $L_{r,app}$, the process of (21) is necessary for both magnitude and phase method to obtain the desired RTC

$$\tau_r = \frac{L_{r,app}}{L_{r,dyn}}\tau_{r,dyn}. \tag{21}$$

The block diagram of the proposed method is shown in Fig. 4. The magnitude method only needs the ac component of λ^m_{dr}, and the magnitude response is obtained by (15). Sequentially, the estimated RTC $\tau_{r,mag}$ is acquired by (21) after the dynamic RTC is estimated by (17). The phase method calculates the phase response with the ac components of the magnetic flux by (18), followed by (20) and (21), estimating $\tau_{r,phase}$.

B. Error Analysis in the Proposed Method

This section analyzes the impact of the parameter error in the proposed method. There are primary estimation errors of $\hat{\lambda}^m_{ds}$ and parameter errors of σL_s and L_m. The estimation error of $\hat{\lambda}^m_{ds}$ is caused by the stator resistance R_s, which makes FAO erroneous. In the experiment, σL_s and L_m are obtained experimentally, with estimation errors. The first case in Fig. 5(a) assumes the inaccurate stator resistance R_s, which leads to FAO error, and the other parameters are assumed to be accurate. Likewise, the second case in Fig. 5(b) assumes the inaccurate transient

inductance σL_s, and the other parameters are assumed to be accurate. Meanwhile, the rotor resistance R_r is unknown for the overall proposed method.

Once the current I_{dc} and I_{ac} are determined in (13), the magnetic flux magnitude A and B are determined, the stator magnetic flux phase θ is determined, and γ', calculated by the inductance, is determined. The errors in $\hat{\lambda}_{ds}^{m}$ and σL_s make the magnitude and phase response erroneous by changing A to lA and B to mB as shown in Fig. 5. The other variables are kept constant and decided by the current magnitude.

The case when $\hat{\lambda}_{ds}^{m}$ is inaccurately estimated is shown in Fig. 5(a). Compared with the correctly estimated case, if $\hat{\lambda}_{ds}^{m}$ is estimated to be l times bigger, k becomes bigger by (15), and ϕ becomes smaller by (18). In this case, the k_1 and ϕ_1 are shown as follows:

$$k_1 = \frac{1}{\gamma' I_{ac}} \left|\left| \lambda_{dr,1}^{m'} \right|\right| = \frac{1}{\gamma' I_{ac}} \sqrt{(lA\cos\theta - B)^2 + (lA\sin\theta)^2} \tag{22}$$

$$\phi_1 = \tan^{-1}\left(\frac{lA\sin\theta}{lA\cos\theta - B}\right). \tag{23}$$

If $\hat{\lambda}_{ds}^{m}$ is estimated to be 10% bigger based on (22) and (23), the estimation error of the RTC is shown in Fig. 6(a) depending on the frequency of the applied ac component. The ϕ is more robust to $\hat{\lambda}_{ds}^{m}$ error than k. Likewise, if σL_s is estimated to be m times bigger, k becomes smaller, and ϕ becomes bigger as shown in Fig. 5(b) as follows:

$$k_2 = \frac{1}{\gamma' I_{ac}} \left|\left| \lambda_{dr,2}^{m'} \right|\right| = \frac{1}{\gamma' I_{ac}} \sqrt{(A\cos\theta - mB)^2 + (A\sin\theta)^2} \tag{24}$$

$$\phi_2 = \tan^{-1}\left(\frac{A\sin\theta}{A\cos\theta - mB}\right). \tag{25}$$

When σL_s is estimated to be 30% bigger, the estimation error of the RTC appears as shown in Fig. 6(b). Both methods are not sensitive to the error of σL_s.

Lastly, if there is an error in L_m, as shown in (15) and (18), the effect of the error appears only on k because the value of L_m is not needed for the ϕ calculation process. When there is a 10% error in L_m, the RTC estimation method based on k is sensitive to the operating frequency, as shown in Fig. 6(c).

Fig. 6 shows the analysis of the RTC estimation errors of the two methods at a rated magnetizing current of 3.7 kW IM. In Fig. 6, the errors are plotted against the test frequency ω_o. The test frequency is normalized by ω_c, which determines the dynamics of λ_{dr}^{m} to i_s as shown in (12). As shown in (16) and (19), the normalized test frequency ω_o/ω_c decides the magnitude and phase response.

In conclusion, analyzing the effect of errors on the three variables, it can be determined that though the motor parameters affect both the magnitude and phase method, estimating the RTC using the phase method will be more robust to estimation errors than using the magnitude method. If the current magnitude changes, the calculated error will change, but the same conclusion will be drawn: the phase method is more robust than the magnitude method.

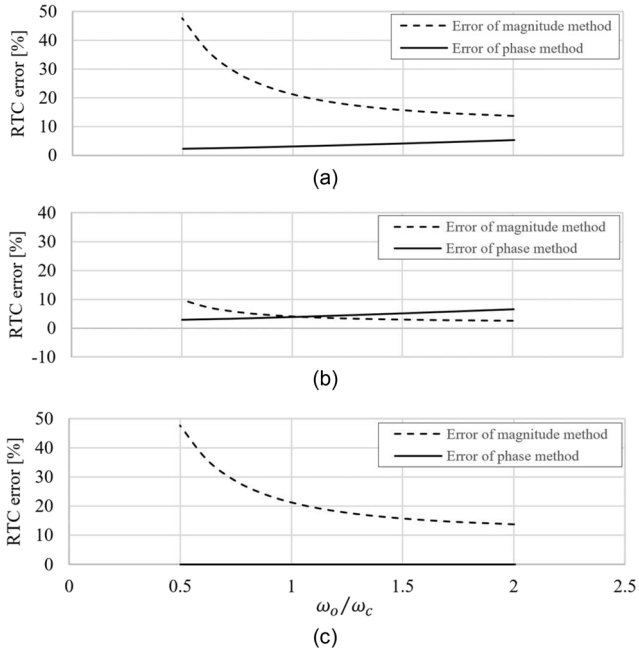

Fig. 6. Comparison of the RTC estimation error with respect to the frequency. (a) 10% error in the estimated stator magnetic flux. (b) 30% error in transient inductance. (c) 10% error in magnetizing inductance.

TABLE I
DATA OF THE 3.7 kW IM

Parameter	Value [Unit]
Rated power	3.7 [kW]
Rated voltage	380 [V]
Rated current	8.4 [A]
Pole number	4 poles
Rated torque	19.6 [Nm]
Rated speed	1745 [r/min]
Stator resistance	1.152 [Ω]
Rotor resistance	1.008 [Ω]
Magnetizing inductance	199.6 [mH]
Leakage inductance	17.6 [mH]

IV. Simulation and Experimental Results

The FAO [20] is used to estimate the stator magnetic flux. The observation frequency of the FAO is selected, and the output of the FAO is analyzed in [21] to reduce the estimation error. The detailed explanation is in Appendix I.

A simulation is performed using the PLECS to verify the proposed method. The motor used in the simulation is a 3.7 kW squirrel cage IM, and the nameplate parameters of IM are shown in Table I. The switching frequency and sampling frequency are 10 kHz, the current controller bandwidth is 250 Hz, and the dc link voltage is 540 V. The IM model used in the simulation considers the magnetic saturation of magnetizing inductance, and

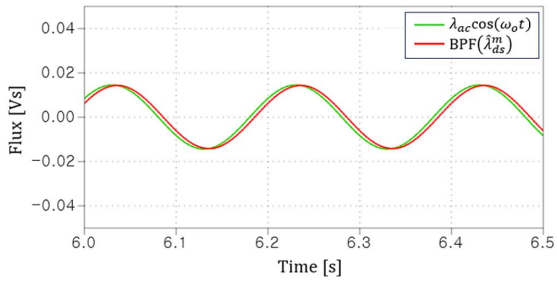

Fig. 7. AC component of the stator magnetic flux and the ac component of the estimated magnetic flux extracted by BPF at 5 Hz.

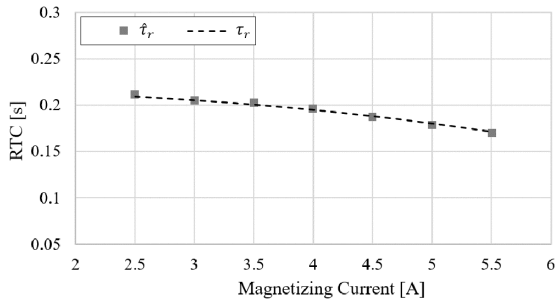

Fig. 8. Simulation result at various stator currents.

the magnetic flux saturation model is a function of current with respect to the magnetic flux. The magnetic flux saturation model of the magnetizing flux and fitted coefficients used for simulation is attached in Appendix II and Table A-I. Additionally, the transient inductance σL_s is assumed to be a constant in simulation.

In the experiment, the dc-link voltage of the inverters and the phase current of both M-G motors are measured with sensors. The inverters are controlled by TMS320F28377S control board.

A. Simulation Results

The IM is I-F driven by the dc magnetizing current, and the proposed method begins with adding the ac signal with operating frequency. The magnitude of ac signal is 10% of the dc current.

At first, the analysis in (A4) and (A5) is confirmed with the simulation. Fig. 7 is a waveform of the estimated stator magnetic flux through FAO and the actual stator magnetic flux. As mentioned at the beginning of Section IV, the estimated magnetic flux from FAO lags to the actual magnetic flux, and the magnitude decreases when the ac component is extracted with band-pass filter (BPF). According to the simulation, when the operating frequency of the ac signal is 5 Hz, the magnitude reduction ratio η and phase difference δ are approximately 0.984 and $-10.1°$, respectively. In comparison, the values predicted through (A4) and (A5) were 0.985 and $-9.9°$, respectively. The values of η and δ from (A4) and (A5) are similar to the simulation result.

Fig. 8 shows the estimated RTC at an operating frequency of 1.75 Hz compared with the RTC according to magnetizing current. The operating frequency is selected near the rated slip frequency. As the magnetizing current increases, the magnetizing inductance is saturated, and the RTC tends to decrease. As a result of estimating the RTC according to the proposed method, the estimation error rate was up to 0.7%, which is a reasonable estimate.

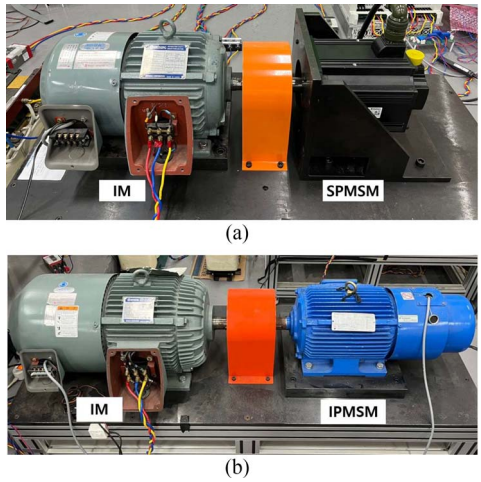

Fig. 9. Motor-generator set. (a) 3.7 kW IM. (b) 11 kW IM.

TABLE II
DATA OF THE 11 KW IM

Parameter	Value [Unit]
Rated power	11 [kW]
Rated voltage	220 [V]
Rated current	45 [A]
Pole number	4 poles
Rated torque	58.3 [N· m]
Rated speed	1750 [r/min]
Stator resistance	0.105 [Ω]
Rotor resistance	0.0645 [Ω]
Magnetizing inductance	23.49 [mH]
Leakage inductance	2.118 [mH]

B. Experimental Results

To verify the proposed method under the various motor environment which has different magnetic saturation, 3.7 and 11 kW IM are used to verify the proposed method experimentally. The test motor and the load motor are shown in Fig. 9. The motor parameters of the 11 kW IM used for the experimental verification are shown in Table II. The nominal stator resistance is kept constant and rotor resistance is assumed unknown. The stator magnetic flux according to the stator current is obtained experimentally. Then, the magnetic flux saturation model of the stator magnetic flux in (A6) is used, and coefficients of the saturation model are obtained with the MATLAB curve fitting tool. The coefficients are shown in Table A-II. The subscript m, which represents magnetizing flux and current, is changed to s, which represents stator magnetic flux and current. The experimental data and fitted model are shown in Fig. A1. As shown in Fig. A1, the error between the experimental data and the fitted model is negligible, which makes the inductance calculation reliable.

Although the transient inductance σL_s kept constant in simulation, it appears the magnetic saturation [23]. In the experiment,

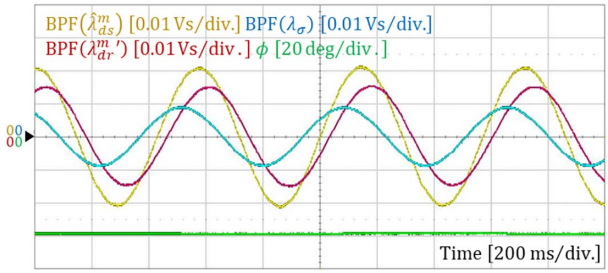

Fig. 10. Waveform of the magnetic flux at rated magnetizing current, 3.7 kW IM.

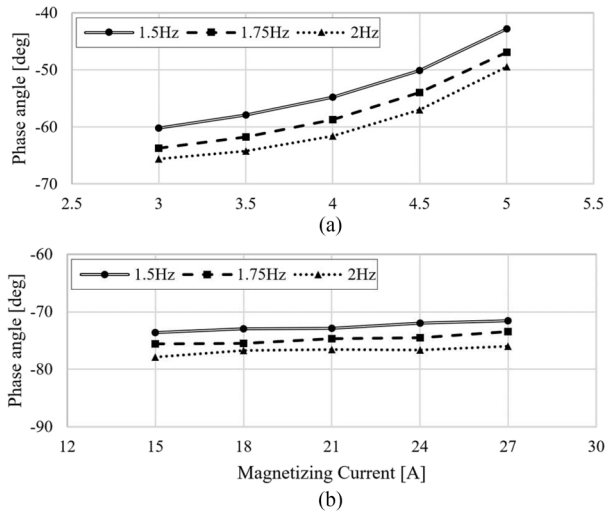

Fig. 11. Phase angle of λ^m_{dr} with respect to the magnetizing currents and the operating frequencies. (a) 3.7 kW IM. (b) 11 kW IM.

the transient inductance is obtained experimentally by considering the rated slip frequency is shown in Fig. A2.

Fig. 10 is the experimental waveform when the operating frequency is 1.75 Hz. The estimated stator magnetic flux lags the leakage magnetic flux as shown in Fig. 3. The rotor magnetic flux of inverse Γ model $\lambda^{m'}_{dr}$ is calculated by subtracting two magnetic fluxes shown as (12).

Fig. 11 shows the phase response angle at 3.7 and 11 kW IM and the estimated RTC on the experiment. Under the same operating frequency, as the magnetizing current increases, magnetizing inductance L_m decreases due to the magnetic flux saturation. If the RTC decreases, the cutoff frequency ω_c increases, increasing phase response angle ϕ at the same operating frequency.

From Fig. 11(a), the phase response angle of 3.7 kW IM significantly increases as the current increases. However, as shown in Fig. 11(b), the phase increment by the current increase in 11 kW IM is relatively small under the same operating frequency. The distinction is caused by the difference in the two IMs' magnetic saturation models. The phase angle is used to calculate $\tau_{r,phase,dyn}$ by (20), then converted to $\tau_{r,phase}$ by (21), using $L_{r,app}/L_{r,dyn}$ ratio. According to the fitted magnetic saturation model in Fig. A1, the ratio of 3.7 kW IM varies significantly compared with the 11 kW IM.

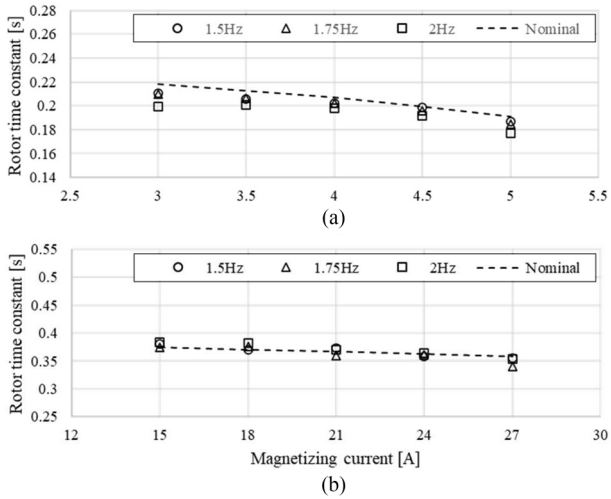

Fig. 12. Experimental results of the estimated RTC at various magnetizing currents. (a) 3.7 kW IM. (b) 11 kW IM.

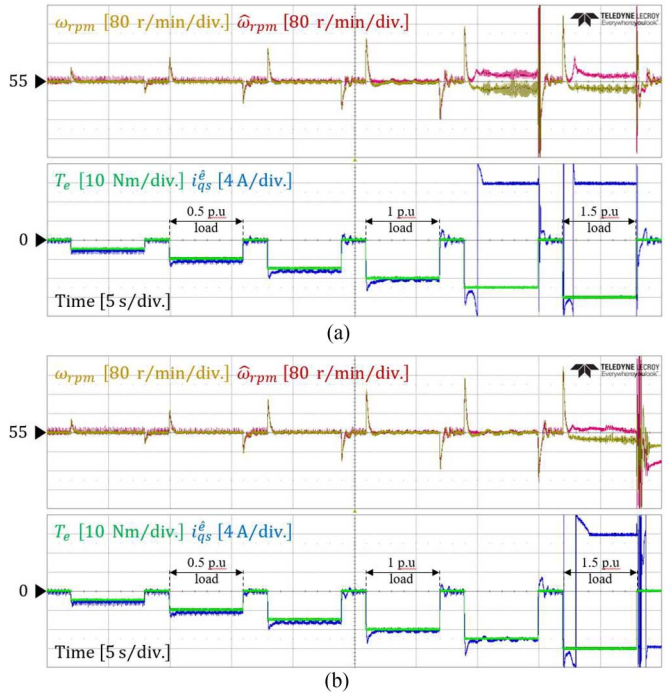

Fig. 13. Sensorless control experiments of 3.7 kW IM with step load. (a) Nominal RTC at rated magnetizing current. (b) Estimated RTC by proposed method at rated magnetizing current.

From Fig. 11(a) and 11(b), the phase response angle decreases as the operating frequency increases under the same magnetizing current. The phase angle changes due to the analysis in (12) by the first-order LPF relationship between the stator current and the rotor magnetic flux.

Fig. 12 shows the estimated RTC using the phase response in Fig. 11. To validate the result, the nominal RTCs at rated magnetizing current of each IMs (4 A, 21 A) are obtained using the auto-tuning of a commercial inverter (LS ELECTRIC: iS7) with the position sensor. At the other currents, the RTCs are calculated as

$$\tau_{rn,x} = \frac{L_{r,x}}{L_{r,rated}} \tau_{rn,rated} \tag{26}$$

where $\tau_{rn,x}$ is nominal RTC at x A and $L_{r,x}$ is the rotor inductance at x A. The $L_{r,x}$ is obtained using the magnetic saturation model in (A6) and Fig. A1, considering the magnetic saturation of the rotor inductance.

The nominal RTC variance due to temperature and slip frequency is neglected since the proposed method operates only in a short period with the rated magnetizing current, and only the no-load condition is regarded. As a result, the RTCs at each current are assumed to be only a variable of the current. As the magnetizing current increases, the nominal RTC decreases due to the magnetic saturation. The trend of the estimated RTC through the proposed method is similar to the nominal RTC values.

Fig. 13 shows the step load test result at a rated slip speed of 3.7 kW IM during sensorless control [25]. Fig. 13(a) is implemented with the nominal RTC, and Fig. 13(b) is implemented with the estimated RTC by the proposed method at the rated magnetizing current. The step load is sequentially increased by 0.25 p.u. Both experiments maintain stability under step load over 1 p.u. Compared with the nominal RTC, the experiment with estimated RTC can withstand 1.25 p.u.

V. Conclusion

This article proposed a method to estimate the RTC during I-F operation in a rotating state. The stator current is controlled by adding an ac signal injected additionally with the dc signal for magnetization conditions. The stator magnetic flux is obtained by the FAO and estimate the RTC using the relationship between the stator current and the rotor magnetic flux. The phase response of the rotor magnetic flux was calculated with the magnitude of the stator and leakage magnetic flux to avoid the inaccuracy of phase extraction. The sensitivity to errors of the two RTC estimation method were analyzed, the method based on the magnitude response of the rotor magnetic flux and based on the phase response. The estimation error was analyzed to be small with the proposed method, based on phase response. The practical issues with the magnetic flux obtained by FAO were analyzed and compensated appropriately. It was confirmed that the estimated RTC with the proposed method was similar to the nominal value of the RTC. The load test with the estimate RTC showed the sensorless control stability up to 1.25 p.u. load. The proposed method was verified through the simulation and experiments.

Appendix I

The transfer function of the FAO [20] is defined as

$$\frac{\hat{\lambda}_s}{\lambda_s} = \frac{2\zeta|\omega_{FAO}|s}{s^2 + 2\zeta|\omega_{FAO}|s + \omega_{FAO}^2} \tag{A1}$$

where $\hat{\lambda}_s$ is the estimated magnetic flux, λ_s is the actual magnetic flux, ζ is the damping ratio of the FAO, and ω_{FAO} is an observation frequency.

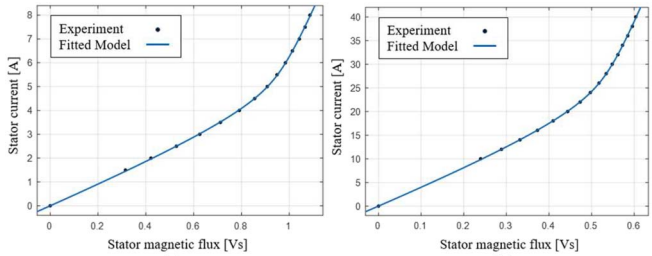

Fig. A1. Experiment data and magnetic saturation model of stator magnetic flux to the stator current. (a) 3.7 kW IM. (b) 11 kW IM.

TABLE A-I
Saturation Model Coefficients in Simulation

Parameter	$L_{m,0}$	$L_{m,\text{sat}}$	λ_T	f_T
Value	0.2145	0.03137	0.9229	2.025

TABLE A-II
Saturation Model Coefficients in Experiments

	Parameter	$L_{s,0}$	$L_{s,\text{sat}}$	λ_T	f_T
Value	3.7 kW IM	0.2228	0.03969	0.9641	2.123
	11 kW IM	0.0255	0.00421	0.5381	1.919

The input of the FAO is expressed as follows:

$$i_s^s = I_{dc} e^{(\omega_{IF} t)\mathbf{J}} + \frac{1}{2} I_{ac} \left(e^{(\omega_p t)\mathbf{J}} + e^{(\omega_n t)\mathbf{J}}\right) \tag{A2}$$

where $\omega_p = \omega_{IF} + \omega_o$, $\omega_n = \omega_{IF} - \omega_o$, and ω_{IF} is I-F operation frequency.

The stator magnetic flux λ_{ds}^m and estimated from FAO $\hat{\lambda}_{ds}^m$ differ in the magnitude and the phase [21]. The magnitude and phase difference between λ_{ds}^m and $\hat{\lambda}_{ds}^m$ should be adequately compensated to obtain the stator magnetic flux correctly.

As shown in (A2), since the stator current includes both dc and ac signals, the observed magnetic flux also includes both dc and ac components. Therefore, the magnitude of the ac component of $\hat{\lambda}_{ds}^m$ is obtained using a BPF, and the magnitude and phase difference due to the BPF also occurs as

$$\hat{\lambda}_{ds,ac}^m = \eta \cdot \lambda_{ac} \cos(\omega_o t + \delta) \tag{A3}$$

where $\hat{\lambda}_{ds,ac}^m$ is ac component of $\hat{\lambda}_{ds}^m$, extracted by using BPF.

If the observation frequency ω_{FAO} is selected as $\sqrt{\omega_p \omega_n}$, the magnitude reduction ratio η and phase difference δ by the FAO and BPF can be calculated as (A4) and (A5) [21]

$$\eta = \frac{2\zeta\omega_{FAO}\omega_p}{\sqrt{\left(\omega_{FAO}^2 - \omega_p^2\right)^2 + \left(2\zeta\omega_{FAO}\omega_p\right)^2}} \tag{A4}$$

$$\delta = \tan^{-1}\left(\frac{\omega_{FAO}^2 - \omega_p^2}{2\zeta\omega_{FAO}\omega_p}\right) = \tan^{-1}\left(\frac{-\omega_o}{2\zeta\omega_{FAO}}\right). \tag{A5}$$

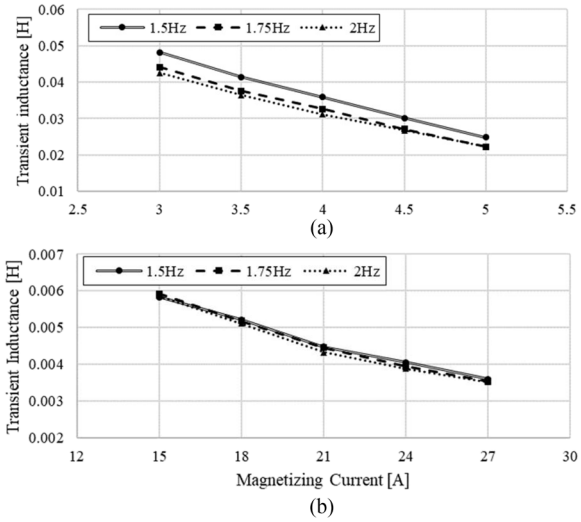

Fig. A2. Experimentally estimated value of σL_s. (a) 3.7 kW IM. (b) 11 kW IM.

The damping ratio ζ is selected as $1/\sqrt{2}$, considering the stability of FAO. Using the analysis of (A4) and (A5), i_s is compensated appropriately.

Appendix II

The magnetic flux saturation model used for simulation and experimental verification is expressed as (A6) [24]

$$i_m(\lambda_m)=\frac{2M_d}{\pi}\{(\lambda_m-\lambda_T)\tan^{-1}(\tau_T(\lambda_m-\lambda_T))-\lambda_T\tan^{-1}(\tau_T\lambda_T)\}+\frac{M_d}{\pi\tau_T}\left[ln\left(1+\tau_T^2\lambda_T^2\right)-ln\left(1+\tau_T^2(\lambda_m-\lambda_T)^2\right)\right]+M_a\lambda_m \quad \text{(A6)}$$

where $M_d=(M_f-M_i)/2$, $M_a=(M_f+M_i)/2$, $M_f=1/L_{m,sat}$ $M_i=((1)/(L_{m,0})-(1)/(L_{m,sat})(0.5-\tan^{-1}(\tau_T\lambda_T)/\pi))/(0.5+\tan^{-1}(\tau_T\lambda_T)/\pi)$, $\tau_T=(f_T/\lambda_T)(L_{m,0}/L_{m,sat})$, i_m is magnetizing current, and λ_m is magnetizing flux.

References

[1] S. Suwankawin and S. Sangwongwanich, "Design strategy of an adaptive full-order observer for speed-sensorless induction-motor drives-tracking performance and stabilization," *IEEE Trans. Ind. Electron.*, vol. 53, no. 1, pp. 96–119, Feb. 2006.

[2] A. Yoo, S. Han, Y. I. Son, Y. Yoon, and C. Hong, "Gain design of an adaptive full-order observer using a pole placement technique for speed sensorless induction motor drives," *J. Power Electron.*, vol. 16, no. 4, pp. 1346–1354, 2016.

[3] Y.-D. Yoon and S.-K. Sul, "Sensorless control for induction machines based on square-wave voltage injection," *IEEE Trans. Power Electron.*, vol. 29, no. 7, pp. 3637–3645, Jul. 2014.

[4] L. Tiitinen, M. Hinkkanen, and L. Harnefors, "Speed-adaptive full-order observer revisited: closed-form design for induction motor drives," in *Proc. IEEE Int. Symp. Sensorless Control Elect. Drives (SLED)*, Seoul, Republic of Korea, 2023, pp. 1–6.

[5] M. Hinkkanen, L. Harnefors, and J. Luomi, "Reduced-order flux observers with stator-resistance adaptation for speed-sensorless induction motor drives," in *Proc. IEEE Energy Convers. Congr. Expo.*, San Jose, CA, USA, 2009, pp. 155–162.

[6] B. Karanayil, M. F. Rahman, and C. Grantham, "Online stator and rotor resistance estimation scheme using artificial neural networks for vector controlled speed sensorless induction motor drive," *IEEE Trans. Ind. Electron.*, vol. 54, no. 1, pp. 167–176, Feb. 2007.

[7] S. Foti, A. Testa, S. De Caro, T. Scimone, and M. Pulvirenti, "Rotor flux position correction and parameters estimation on sensorless multiple induction motors drives," *IEEE Trans. Ind. Appl.*, vol. 55, no. 4, pp. 3759–3769, Jul./Aug. 2019.

[8] Y. Park and S.-K. Sul, "Implementation schemes to compensate for inverter nonlinearity based on trapezoidal voltage," *IEEE Trans. Ind. Appl.*, vol. 50, no. 2, pp. 1066–1073, Mar./Apr. 2014.

[9] H. A. Toliyat, E. Levi, and M. Raina, "A review of RFO induction motor parameter estimation techniques," *IEEE Trans. Energy Convers.*, vol. 18, no. 2, pp. 271–283, Jun. 2003.

[10] E. Mölsä, L. Tiitinen, S. E. Saarakkala, L. Peretti, and M. Hinkkanen, "Standstill identification of an induction motor model including deep-bar and saturation characteristics," *IEEE Trans. Ind. Appl.*, vol. 57, no. 5, pp. 4924–4932, Sep./Oct. 2021.

[11] J.-H. Lee and S.-K. Sul, "Inverter nonlinearity compensation of discontinuous PWM considering voltage drop of power semiconductor and dead time effect," in *Proc. IEEE Energy Convers. Congr. Expo. (ECCE)*, Detroit, MI, USA, 2020, pp. 5677–5682.

[12] L. Peretti and M. Zigliotto, "Automatic procedure for induction motor parameter estimation at standstill," *IET Electr. Power Appl.*, vol. 6, no. 4, pp. 214–224, Apr. 2012.

[13] C. Sukhapap and S. Sangwongwanich, "Auto tuning of parameters and magnetization curve of an induction motor at standstill," in *Proc. IEEE Int. Conf. Ind. Technol.*, Bangkok, Thailand, vol. 1, 2002, pp. 101–106.

[14] N. R. Klaes, "Parameter identification of an induction machine with regard to dependencies on saturation," *IEEE Trans. Ind. Appl.*, vol. 29, no. 6, pp. 1135–1140, Nov./Dec. 1993.

[15] S. Khamehchi, E. Mölsä, and M. Hinkkanen, "Comparison of standstill parameter identification methods for induction motors," in *Proc. IEEE Symp. Sensorless Control Elect. Drives,* Helsinki, Finland, Sep. 2018, pp. 156–161.

[16] J. W. Choi, S. I. Yong, and S. K. Sul, "Inverter output voltage synthesis using novel dead time compensation," in *Proc. IEEE Appl. Power Electron. Conf. Expo. (ASPEC)*, Orlando, FL, USA, 1994, pp. 100–106.

[17] D. Chatterjee, "A simple leakage inductance identification technique for three-phase induction machines under variable flux condition," *IEEE Trans. Ind. Electron.*, vol. 59, no. 11, pp. 4041–4048, Nov. 2012.

[18] H. A. Toliyat, M. S. Arefeen, K. M. Rahman, and D. Figoli, "Rotor time constant updating scheme for a rotor flux-oriented induction motor drive," *IEEE Trans. Power Electron.*, vol. 14, no. 5, pp. 850–857, Sep. 1999.

[19] A. Yoo, C. Hong, and J.-I. Ha, "On-line rotor time constant estimation for indirect field oriented induction machine," in *Proc. IEEE Energy Convers. Congr. Expo.*, Denver, CO, USA, 2013, pp. 3860–3865.

[20] Y. Park, H.-S. Kim, and S.-K. Sul, "Frequency-adaptive observer to extract AC coupled signals for grid synchronization," *IEEE Trans. Ind. Appl.*, vol. 53, no. 1, pp. 273–282, Jan. 2017.

[21] Y.-J. Oh, Y.-D. Yoon, C.-O. Hong, and S.-C. Choi, "Estimation technique for rotor time constant of induction machines during I/f speed control," in *Proc. 11th Int. Conf. Power Electron. ECCE Asia (ICPE)*, Jeju Island, Republic of Korea, 2023, pp. 1088–1094.

[22] G. R. Slemon, "Modelling of induction machines for electric drives," *IEEE Trans. Ind. Appl.*, vol. 25, no. 6, pp. 1126–1131, Nov./Dec. 1989.

[23] E. Mölsä, S. E. Saarakkala, M. Hinkkanen, A. Arkkio, and M. Routimo, "A dynamic model for saturated induction machines with closed rotor slots and deep bars," *IEEE Trans. Energy Convers.*, vol. 35, no. 1, pp. 157–165, Mar. 2020.

[24] K. A. Corzine, B. T. Kuhn, S. D. Sudhoff, and H. J. Hegner, "An improved method for incorporating magnetic saturation in the q-d synchronous machine model," *IEEE Trans. Energy Convers.*, vol. 13, no. 3, pp. 270–275, Sep. 1998.

[25] A. Yoo, C. Hong, and Y.-d. Yoon, "Sensorless torque control of induction machine in low speed and low torque region," in *Proc. 16th Eur. Conf. Power Electron. Appl.*, Lappeenranta, 2014, pp. 1–8.

Ho-Ryul Park (Student Member, IEEE) was born in Gyeonggi-do, South Korea. He received the B.S. degree in automotive engineering in 2022, from Hanyang University, Seoul, South Korea, where he is currently working toward the M.S. degree in automotive engineering.

His research interests include power electronics and control of electric machines.

Yun-Jai Oh received the B.S. degree from Kookmin University, Seoul, Korea, in 2021 and the M.S. degree from Hanyang University, Seoul, Korea, in 2023, both in automotive engineering.

His research interests include electric machine drive system and sensorless drive system. His research interest also includes research on techniques for estimating the parameters of electric machines.

Seok-Min Bae was born in Mokpo, South Korea, in 1997. He received the B.S degree in electrical engineering from Kwangwoon University, Seoul, South Korea, in 2022 and the M.S degree in future mobility from Hanyang University, Seoul, Korea, in 2024.

His research interests include power electronics and control of electric machines.

Seung-Cheol Choi received the B.S. degree from Kangwon National University, Chuncheon, Korea, in 2009 and the M.S. degree from Kunkuk University, Seoul, Korea, in 2011, both in electrical engineering. He is currently working toward the Ph.D. degree in automotive engineering with Hanyang University, Seoul, Korea.

From 2011 to 2019, he was an Engineer with LSIS Company Limited, Anyang, Korea. Since 2021, he has been with LS Electric Company Limited, Anyang. His research interests include power-electronic control of electric machines and high power converter.

Myung-Seop Lim (Senior Member, IEEE) received the bachelor's degree in mechanical engineering from Hanyang University, Seoul, South Korea, in 2012, and the master's and Ph.D. degrees in automotive engineering from Hanyang University, in 2014 and 2017, respectively.

From 2017 to 2018, he was a Research Engineer with Hyundai Mobis, Yongin, South Korea. From 2018 to 2019, he was an Assistant Professor with Yeungnam University, Daegu, South Korea. Since 2019, he has been with Hanyang University, where he is currently an Associate Professor. His research interests include electromagnetic field analysis and multi-physics analysis of electric machinery for mechatronics system such as automotive and robot applications.

Young-Doo Yoon (Senior Member, IEEE) was born in South Korea. He received the B.S., M.S., and Ph.D. degrees in electrical engineering from Seoul National University, Seoul, South Korea, in 2002, 2005, and 2010, respectively.

From 2010 to 2013, he was a Senior Engineer with Samsung Electronics Company, Suwon, South Korea. From 2013 to 2017, he was an Assistant Professor with the Department of Electrical Engineering, Myongji University, Yongin, South Korea. Since 2017, he has been an Associate Professor with the Department of Automotive Engineering, Hanyang University, Seoul, South Korea. His research interests include power electronic control of electric machines, high-power converters, electric vehicles, and electric home appliances.